JOURNAL OF GEOPHYSICAL RESEARCH, VOL. 108, NO. A4, 8019, doi:10.1029/2002JA009701, 2003

Shock aurora: FAST and DMSP observations

X.-Y. Zhou,[1] R. J. Strangeway,[2] P. C. Anderson,[3] D. G. Sibeck,[4] B. T. Tsurutani,[1] G. Haerendel,[5] H. U. Frey,[6] and J. K. Arballo[1]

Received 26 September 2002; revised 4 February 2003; accepted 14 March 2003; published 30 April 2003.

[1] Global signatures of the aurora caused by interplanetary shocks/pressure pulses have been studied in recent years using ultraviolet imager data from polar orbiting spacecraft. The signatures include the occurrence of the aurora first near local noon and then propagation antisunward along the auroral oval at very high speeds. To better understand the mechanisms of particle precipitation, in this paper we study shock auroras using near-Earth observations of the FAST and DMSP satellites. We have studied the events that occurred during 1996–2000 where FAST and/or DMSP crossed the dawnside or duskside auroral zone within 10 min after shocks/pressure pulses arrived at the nose of the magnetopause. It is found that the electron precipitation increased significantly above the dawnside and duskside auroral oval zone after the shock/pressure pulse arrivals. The precipitation structure is low-energy electrons (<~1 keV) at higher latitudes (~75°–83° ILAT within 0600–0900 MLT) and high-energy electrons (~1–10 keV) at lower latitudes (~65°–79° ILAT) of the auroral zone. There are a few degrees (1°–4° ILAT) of overlap between these two categories of precipitated electrons. The precipitation of low-energy electrons was along highly structured field-aligned currents. The precipitation of the high-energy electrons was highly isotropic filling the loss cone. Possible mechanisms of field-aligned current generation are some dynamic processes occurring on the dayside magnetopause, such as magnetic shearing, magnetopause perturbation, magnetic reconnection, and Alfvén wave generation. Adiabatic compression might have caused the high-energy electron precipitation. On the basis of observations of FAST and DMSP, shock auroras are speculated to be diffuse auroras at the lower latitudes of the dayside auroral oval and discrete auroras on the poleward boundary of the oval with a few latitude degree overlap of the two types of auroras. *INDEX TERMS:* 2704 Magnetospheric Physics: Auroral phenomena (2407); 2724 Magnetospheric Physics: Magnetopause, cusp, and boundary layers; 2455 Ionosphere: Particle precipitation; 2784 Magnetospheric Physics: Solar wind/magnetosphere interactions; 2731 Magnetospheric Physics: Magnetosphere—outer; *KEYWORDS:* solar wind-magnetosphere-ionosphere interaction, auroras, particle precipitation

Citation: Zhou, X.-Y., R. J. Strangeway, P. C. Anderson, D. G. Sibeck, B. T. Tsurutani, G. Haerendel, H. U. Frey, and J. K. Arballo, Shock aurora: FAST and DMSP observations, *J. Geophys. Res.*, *108*(A4), 8019, doi:10.1029/2002JA009701, 2003.

1. Introduction

[2] Shock auroras, which are caused by interplanetary shocks or solar wind ram pressure pulses, are one of the most significant visible indications of the dynamic processes in the dayside geospace. The auroral intensity can be 10 kR or higher at ultraviolet wavelengths (see Figure 1). Shock auroras have been identified in ultraviolet images by Dynamics Explorer 1 (DE1), Polar UVI and IMAGE FUV [*Craven et al.*, 1986; *Sitar et al.*, 1998; *Spann et al.*, 1998; *Sibeck et al.*, 1999; *Zhou and Tsurutani*, 1999; *Brittnacher et al.*, 2000; *Vorobjev et al.*, 2001; *Frey et al.*, 2002]. The global signatures of a shock aurora is that the aurora first brightens near local noon in the auroral zone, and then propagates antisunward along the auroral oval at very high ionospheric speeds, i.e., ~6 to 11 km s^{-1} [*Zhou and Tsurutani*, 1999], which are much faster than the typical auroral speeds of <1 km s^{-1} [*Vorobjev et al.*, 1975; *Murphree et al.*, 1990]. Before this observation of the high-speed propagation, the first report on interplanetary shocks creating dayside aurora is by *Brown et al.* [1961]. X-ray burst observed from a balloon near ~14 local time indicated enhanced auroral activity [*Brown et al.*, 1961]. Auroral observations from ground-based meridian-scanning photometer (MSP) and all-sky camera at Longyearbyen, Swalbard showed that the entire sky suddenly brightened at a storm sudden commencement (SSC) event that was caused by an interplanetary shock on 29 December 1981 [*Egeland*

[1]Jet Propulsion Laboratory, Pasadena, California, USA.
[2]Institute of Geophysics and Planetary Physics, University of California, Los Angeles, California, USA.
[3]The Aerospace Corporation, Los Angeles, California, USA.
[4]NASA Goddard Space Flight Center, Greenbelt, Maryland, USA.
[5]International University of Bremen, Bremen, Germany.
[6]Space Science Laboratory, University of California, Berkeley, California, USA.

0148-0227/03/2002JA009701$09.00

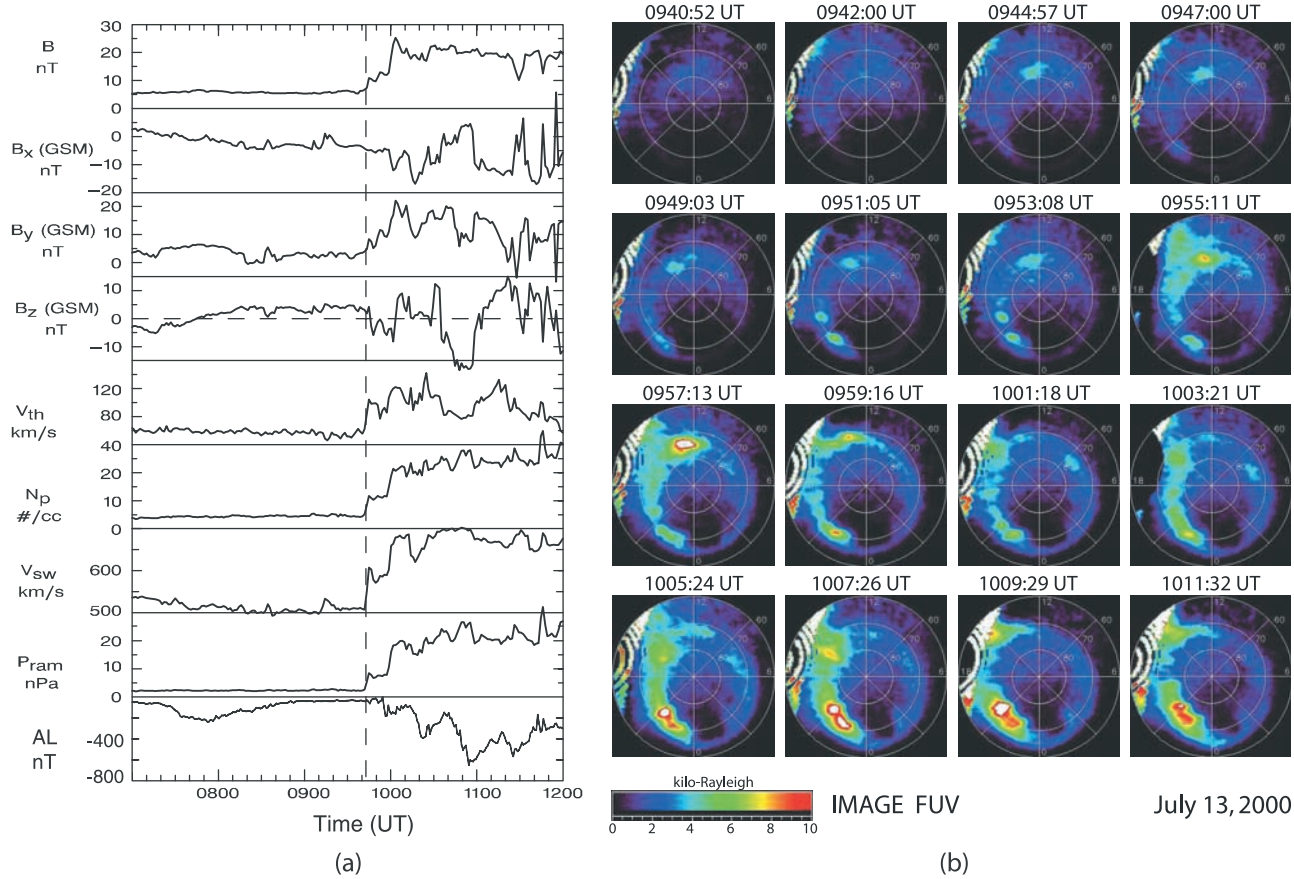

Figure 1. (a) Wind observations and AL index for the 13 July 2000 interplanetary shock event. (b) Shock aurora observed by the IMAGE-FUV WIC instrument at the far ultraviolet wavelength of 140–180 nm [*Mende et al.*, 2000]. The aurora is shown in geomagnetic latitude/MLT coordinates. In each image the magnetic pole is at the center, magnetic local noon is at the top, and dawn is on the right. The time sequence goes from left to right, then down to the next row. The image cadence is ~2 min.

et al., 1994]. With 12 min temporal resolution, space observations from ultraviolet imaging photometers onboard DE1 showed that the entire auroral oval brightened after SSC events [*Craven et al.*, 1986]. Cusp auroras occurred and became very intense after a SSC event on 30 November 1997 when the IMF was strongly northward [*Sandholt et al.*, 2002].

[3] As a significant ionospheric indication of the solar wind-magnetospheric interaction under intense solar wind ram pressure conditions, shock aurora is not only a manifestation of various physical processes on the magnetopause boundary layer, but also a manifestation of the severely compressed magnetosphere. Magnetopause processes include magnetic reconnection, waves and plasma transport, which have been extensively discussed in the special section "Physics of the Magnetopause" in *Journal of Geophysical Research*, *100*(A7), 11,805, 1995, and two AGU *Geophyscial Monographs* (*Physics of the Magnetopause*, vol. 90, and *Earth's Low-Latitude Boundary Layer*, vol. 133). Some of these processes have been thought to be associated with dayside auroral activities. Such as the dayside magnetic reconnection may cause auroral brightening and its meridional movement [e.g., *Sandholt et al.*, 1989, 1994; *Rairden and Mende*, 1989; *Fasel et al.*, 1992; *Leontyev et al.*, 1992]. Large-scale waves in the low-latitude boundary layer (LLBL) can drive toroidal oscillations of the magnetic field. A possible source mechanism for these waves is the Kelvin-Helmholtz instability [*Miura*, 1992; *Kivelson and Chen*, 1995] driven by solar wind velocity shear interactions with the magnetopause. These oscillations can modulate currents, particles, and auroral patterns [*Bythrow et al.*, 1981; *Lui et al.*, 1989; *Potemra et al.*, 1990; *Vo and Murphree*, 1995]. Magnetopause perturbation caused by solar wind pressure pulses [*Sibeck*, 1990, 1991] may lead to double-vortex and field-aligned current generation and cause dayside auroral intensification [*Southwood and Kivelson*, 1990; *Luhr et al.*, 1996; *Sitar et al.*, 1998; *Sibeck et al.*, 1999]. Magnetic field shearing on the magnetopause boundary layer has been thought to be another mechanism for dayside auroras [*Haerendel*, 1994, 2001; *Tsurutani et al.*, 2001a].

[4] In addition to the above magnetopause processes, high compression of the magnetopause and the outer magnetosphere may also lead to particle precipitation due to lowering of the mirror points of trapped particles to altitudes below 100 km [*Spann et al.*, 1998]. Further studies by *Zhou and Tsurutani* [1999], and *Tsurutani et al.* [2001a, 2001b] have suggested that the adiabatic compression leads to a loss cone instability, wave growth and enhanced pitch angle scattering. Particles might be lost into the loss cone

Table 1. The Six Events That Have FAST Observations

		Wind Observation			FAST Observation				Electron Precipitation
Event Date	SSC, UT	Type	Time, UT	ΔP_{ram}, nPa	Orbit	Time, UT	MLT	Hemisphere	Enhancement
15 July 1997	0311	PP	0250	2	3544	0318–0327	0800–1000	N	yes
4 Aug. 1997	–	PP	0215	4	3760	0232–0244	0600–0900	N	yes
22 Nov. 1997	0949	IS	0912	10	4953	0947–1001	0700–0900	S	yes
4 March 1998	1156	IS	1102	1	6059	1200–1213	0830–1100	N	yes
23 June 2000	1303	IS	1300	6	15218	1307–1313	0920	N	yes
13 July 2000	0942	IS	0944	4	15435	0949–0959	0730	S	yes

and cause auroras. This scenario implies that the shock aurora can occur at very low magnetic latitudes near local noon, for it is this region that maps into the outer magnetosphere near the nose of the magnetopause, which is most intensely compressed as a shock/pressure pulse impinges on the magnetopause. Recently, using the Polar UVI data it has been reported by *Liou et al.* [2002] that shock auroras expand to ~65° magnetic latitude (MLAT) within a region of ~1000–1400 magnetic local time (MLT). Using the IMAGE FUV data from SI-12 instrument, proton auroras were found in similar region [*Zhang et al.*, 2002]. In other events (such as the event shown in Figure 1) the shock aurora expanded to ~60° MLAT at ~14 MLT. Theoretically, shock auroras could occur at any foot points of L shells where there is preexistent plasma that is compressed severely by interplanetary shocks/pressure pulses.

[5] In order to determine the mechanisms of particle precipitation and shock aurora forms, we have studied lower altitude observations from the FAST and DMSP spacecraft. In this paper, we focus on the dawnside and duskside aurora oval crossings. The dawnside auroral oval is defined as a sector of the oval from 0400 to 1100 MLT and the duskside oval is a sector from 1300 to 2000 MLT. We will discuss several shock aurora events during which the data from FAST, DMSP, Polar UVI, and IMAGE FUV instruments are available. Mechanisms of the particle precipitation and the possible shock aurora patterns will be discussed.

2. Data Analysis

[6] In this study, SSC events published in the International Service of Geomagnetic Indices (ISGI) monthly bulletins have been used to determine the arrival times of interplanetary shocks. When there are Polar UVI data available, the auroral intensification and propagation are also used as a reference for the identification of shock/pressure pulse arrival times.

[7] We assume that the shock auroras are basically conjugate from the view of the global signature. This is a reasonable assumption based on the mechanisms that were discussed in the Introduction. Therefore Polar UV and IMAGE FUV images for the conjugate Northern Hemisphere aurora have been used for FAST or DMSP satellite passes above the auroral oval in the Southern Hemisphere.

2.1. Criteria for FAST Event Selection

[8] The Fast Auroral SnapshoT (FAST) satellite was launched on 21 August 1996 into an 83°-inclination orbit with an ~2-hour orbital period. The apogee and perigee are at 4200 km and 350 km altitudes, respectively. The FAST satellite was designed to make high time resolution microphysical measurements in the auroral acceleration region. Its spin axis tilts slightly from the orbit normal direction such that the Earth's magnetic field is nearly always within 5° of the spin plane during auroral zone passes. The scientific instruments include a complement of particle and field sensors that are controlled by a single instrument data processing unit. Instruments used in this study are Electrostatic Analyzers (ESAs), Time-of-flight Energy Angle Mass Spectrograph (TEAMS), and magnetic and electric fields sensors (which include both a DC fluxgate magnetometer and an AC search-coil magnetometer). A summary of FAST instruments can be found in the overview paper by *Carlson et al.* [1998].

[9] The criteria for selecting FAST observation events are as follows: (1) the FAST spacecraft crossed the dawnside or duskside auroral oval within 10 min after an interplanetary shock/pressure pulse arrival. (2) Only auroral crossings in the same MLT sector were used for the comparison of data from before and after the shock arrival. This criterion also constrains a comparison to be between consecutive orbits, i.e., the one after the shock arrival and the previous orbit. (3) Since the FAST orbital period is ~2 hr 10 min, an additional restriction has been applied. It is that the solar wind and magnetosphere are quiet during the two and half hour period before interplanetary shocks/pressure pulses arrived at the Earth. This requirement means the dawnside and duskside oval were not contaminated by substorm auroras. The specific requirements that we imposed are that the IMF B_z is greater than −2 nT, or the AL magnitude is less than 300 nT.

[10] For 6 out of 148 SSC events that occurred in 1996–2000, there are FAST passes that fit our criteria. These events are listed in Table 1, in which the Type column shows the solar wind event is an interplanetary shock (IS), or a pressure pulse (PP). The numbers in the Orbit column are for the FAST orbits that crossed the auroral oval after the shock/pressure pulse arrivals. The Time column for FAST observations gives the interval when FAST crossed the oval. In the Hemisphere column, N (or S) means that FAST was in the Northern (or Southern) Hemisphere. The last column shows whether or not there was significant enhancement of electron precipitation after the shock/pressure pulse arrivals. The FAST data include electron and ion observations, DC and AC magnetic and electric fields. Here we mainly study the electron data. All of the events show significant increases of electron precipitation.

2.2. Criteria for DMSP Event Selection

[11] The DMSP (Defense Meteorological Satellite Program) F11–F14 spacecraft fly in sun-synchronous, 99-degree inclination orbits at ~840 km altitude with orbital

Table 2. The Six Events That Have DMSP Observations

		Wind Observation			DMSP Observation				Relative
Event Date	SSC (UT)	Type	Time, UT	ΔP_{ram}, nPa	DMSP Satellite	Time, UT	MLT	Hemisphere	to SSC
15 May 1997	0159	IS	0115	10	F12	0149	0700	S	P
15 May 1997					F10	0204	0930	S	A
10 Dec. 1997	0526	IS	0433	5	F11	0514	1200	N	P
10 Dec. 1997					F14	0532	1200	N	A
6 Jan. 1998	1416	IS	1329	7	F13	1409–1413	0630	N	P
6 Jan. 1998					F14	1418–1422	0830	S	A
6 Jan. 1998					F13	1402	1700	N	P
6 Jan. 1998					F11	1419–1423	1800	N	A
23 April 1998	1825	IS	1723	5	F14	1820	2000	N	P
23 April 1998					F13	1831	1730	S	A
23 April 1998					F12	1815	1100	S	P
23 April 1998					F14	1830	0900	N	A
10 June 1998	1329	PP	1310	5	F12	1328	0740	S	P
10 June 1998					F13	1339	0600	S	A
24 Sept. 1998	2344	IS	2320	14	F12	2342–2345	0830	S	P
24 Sept. 1998					F11	2348–2352	0600	S	A

periods of ~101 min. The Precipitating Energetic Particle Spectrometer (SSJ/4) aboard the DMSP spacecraft measures electrons and ions in 20 energy channels ranging from 30 eV to 31.3 keV at sweep rate of once per second. The sensors are oriented such that their look direction is within a few degrees of the local vertical. Thus at 840 km in the auroral zone, the instruments are always looking within the loss cone. For a complete description of the SSJ/4 sensors, see *Hardy et al.* [1984].

[12] The SSM, designed and built at Goddard Space Flight Center, is a triaxial fluxgate magnetometer that measures the three components of the geomagnetic field vector at a 12 Hz sampling rate. The Z component of the measured magnetic field is down toward the Earth along the local vertical direction. The Y component of the measured field is perpendicular to Z and in the forward direction (the spacecraft's velocity vector when it is perpendicular to Z). The X component of the measured field is in the sense of a right-handed coordinate system. Thus X is toward the nightside of the orbit plane. Therefore a positive gradient in X direction indicates field-aligned currents coming into the ionosphere. SSM data are available from the F12, F13 and F14 satellites. For a more detailed description, see *Rich et al.* [1985].

[13] Criteria for selecting DMSP observation events are as follows: (1) the DMSP satellite crossed the dawnside or duskside auroral oval within 20 min prior to a shock/pressure pulse arrival, and within 10 min after the arrival. (2) For 30 min upstream of shocks/pressure pulses, the solar wind was quiet, and within 30 min before the SSC there was no substorm contaminating the dawnside and duskside auroral oval. Quantitatively, the criteria of IMF $B_z \geq -2$ nT and/or AL ≥ -300 nT were applied in general. (3) Only auroral passes in the same MLT sector are used for data comparison. (4) The solar wind ram pressure increases at shocks/pressure pulses would be $P_{ram} \geq 5$ nPa. The criteria for DMSP events are more constrained than that for the FAST event selection because there are more DMSP satellites available with shorter orbital periods.

[14] For 6 out of 64 SSC events that occurred in 1997–1998, DMSP observations were available. Table 2 gives the detailed information for the 6 events. This table has the same format as Table 1. In the last column, P (A) indicates that the DMSP pass was prior to (after) the SSC.

3. Interplanetary Shock Effects Observed by FAST Above the Auroral Zone

3.1. The 13 July 2000 Event

[15] At ~0943 UT on 13 July 2000, an interplanetary shock arrived at the Wind spacecraft at (−6.6, −56.3, 14.2 R_e) in GSM coordinates. The solar wind conditions and the AL index are shown in Figure 1a. During the first half of 13 July 2000 the solar wind was quiet. The dawnside and duskside portions of the auroral oval were quiet as well. At the time of the interplanetary fast forward shock (as shown by the dashed vertical line) the IMF magnitude increased from ~6 to 11 nT. The B_z component increased from ~2 to 4 nT, then turned southward to ~−6 nT ~3 min after the shock. The solar wind ram pressure ($1.16\rho_p V^2$, assuming of He^{++} density was 4% of proton density) increased from ~2.6 to 8.4 nPa. Another stronger fast forward shock was detected by Wind at ~0958 UT when Wind was at (−3.6, −6.5, −56.3 R_e). This shock caused very intense dayside aurora with intensities ≥10 kR near local noon.

[16] Figure 1b shows the auroral intensification caused by the interplanetary shock. The aurora was detected by the IMAGE FUV imager. The aurora first brightened at ~0943 UT near local noon. At 0947:00 UT, the aurora became brighter, and on the duskside the auroral intensity was ~2–3 kR. The aurora expanded to ~2130 MLT on the duskside, while it peaked at ~0800 MLT on the dawnside. At 0955:11 UT and after, the dayside aurora brightening increased with significant asymmetry with the duskside aurora being brighter than the dawnside which expanded to ~0530 MLT. The auroral intensity near local noon increased to ~9 kR, while the aurora expanded to ~60° MLAT near 14 MLT with a brightening at ~5–6 kR. The dawnside aurora arrived at the region of ~0200 MLT at a intensity of 2–3 kR. After 1005 UT, the aurora within 2000–0000 MLT reached an intensity that was >10 kR while the dayside aurora near noon decayed.

[17] The FAST observations for this event are shown in Figure 2. Figures 2a and 2b show the observations prior to

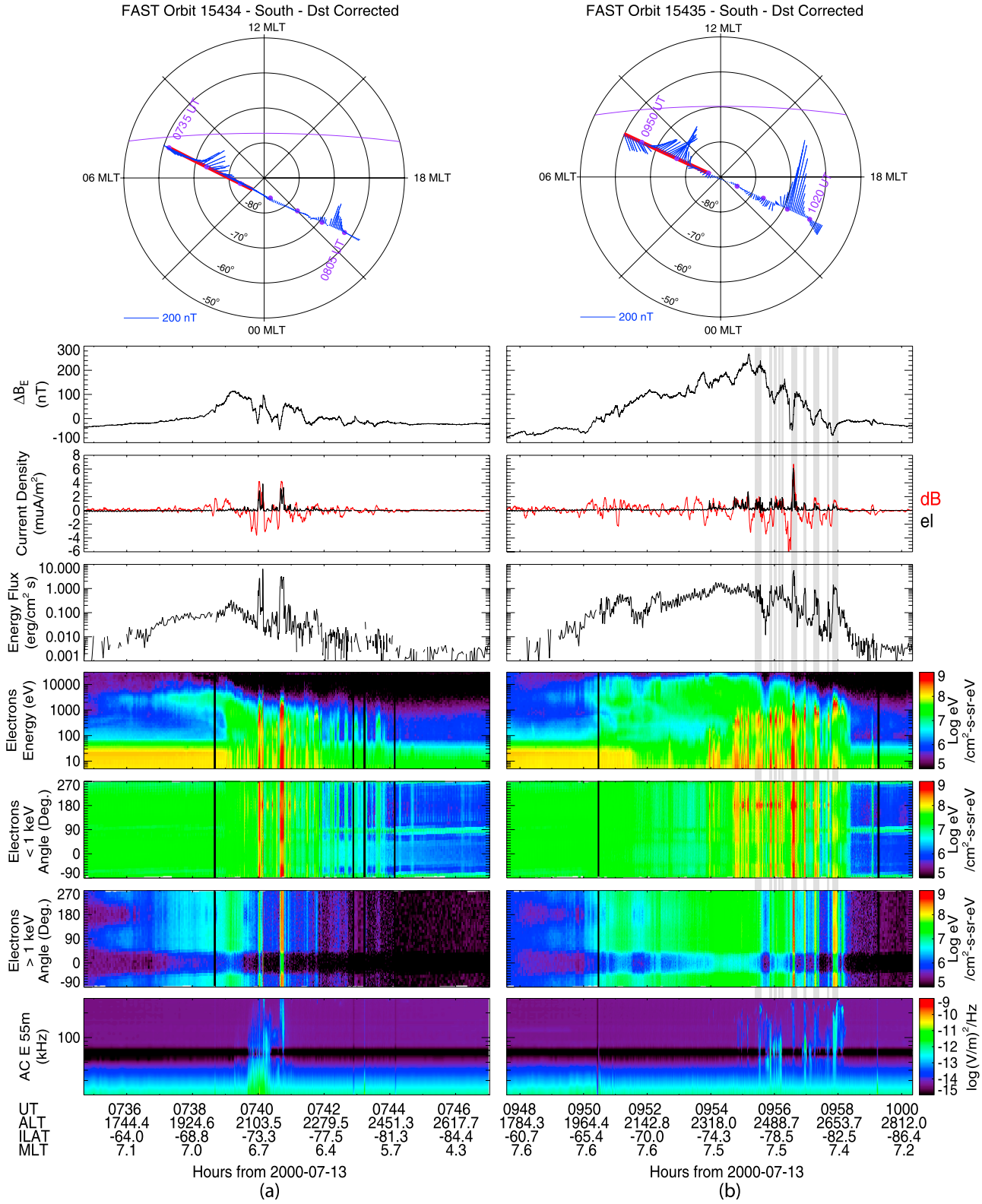

Figure 2. FAST observations for the 13 July 2000 event during a dawnside auroral zone pass in the Southern Hemisphere. FAST was at 2000–2500 km altitude. FAST orbit plots in invariant latitudes are at the top of the figures. The red segments along the orbits are the intervals during which the FAST observations are shown in the panels below the orbit plots. The blue lines projecting from the orbit plots are magnetic field changes. The purple lines show the sunlight termination. Figure 2a shows the observations of orbit 15434 above the auroral oval prior to the shock arrival. Figure 2b shows the observations of orbit 15435 above the auroral oval after the arrival.

and after the shock arrival at ~0942 UT. The top two panels of Figure 2 are FAST orbit plots. FAST crossed the magnetic pole region in the Southern Hemisphere from dawn (on the left) to dusk (on the right). After the shock arrival, the plasma convection increased significantly, as indicated by the increased magnetic field change (blue lines). The red segments along the passes are the intervals of auroral oval crossings during which the FAST observations are shown in the panels below the orbit plots.

[18] In Figure 2a, ΔB_E is the magnetic field perturbation, positive eastward. For a southward spacecraft trajectory (i.e., toward the south pole in the Southern Hemisphere, away from the north pole in the north), as is the case for Figure 2, a positive gradient indicates a field-aligned current away from the ionosphere. Weak upward region 2 and downward region 1 field-aligned currents were detected from ~0738 to 0742 UT. Two upward field-aligned currents, at 0740:05 and 0740:45 UT, were detected in the downward region 1 current as shown by the two peaks in the calculated current densities. We calculated the current densities using two methods as indicated by the red and black traces. The red trace is for the current density obtained from ΔB_E, assuming a sheet-like and stationary field-aligned current, and the black trace is from the number flux of precipitated electrons. By convention, positive current density is along the magnetic field direction, i.e., away from the ionosphere for the Southern Hemisphere, into the ionosphere for the Northern Hemisphere. The two calculations are consistent where there are down going electrons (up going currents).

[19] As shown in the first panel of the FAST observation in Figure 2b, the intensity of the region 1 and 2 field-aligned currents increased significantly after the shock arrival as the change in ΔB_E by ~300 nT. There were highly structured upward field-aligned currents (the vertical shadings where ΔB_E increased abruptly) embedded in the high-latitude downward region 1 currents. Within these upward currents, the current density and the downward electron energy flux abruptly increased (the shadings in the second to the fifth panels). In panel 3, the downward electron energy flux increased about an order of magnitude on average over that shown in Figure 2a. In the fourth panel, the energy spectrum shows that the electron precipitation with electron energy in the region of ~1–10 keV was mainly at the lower latitudes from ~65°–79° ILAT (invariant latitude), which is shown by the fairly constant green background from ~0950 to 0956 UT. These high-energy electrons were highly isotropic and filled the loss cone as shown by the pitch angle distribution in the second panel from the bottom. On the other hand, the electron precipitation with electron energy lower than ~1–2 keV was mainly at the higher latitude region of ~76°–83° ILAT (see the fourth, fifth and sixth panels). These electrons precipitated along field-aligned currents as shown by those intense electron energy beams in the fourth panel. In a region of ~76°–79° ILAT, there is an overlap of high- and low-energy electron precipitation. This is also the boundary between upward region 2 and downward region 1 field-aligned currents as shown by the ΔB_E component.

[20] The right bottom panel of Figure 2 shows that electromagnetic broadband waves were observed with intensity at $\sim 10^{-12}$–10^{-11} V^2 m^{-2} Hz^{-1}. It should be noted that these waves were detected at higher latitudes where the field-aligned currents were (aligned by the vertical shadings). The plasma waves were 4–40 kHz magnetic waves and 2–500 kHz electric emissions, which are polar cap boundary layer waves. It has been reported that the broadband waves in the magnetopause boundary layers are associated with the auroral brightening because the waves are on the magnetic fields mapping into the auroral oval [*Gurnett and Frank*, 1977; *Gurnett et al.*, 1979; *Tsurutani et al.*, 1981; *Lakhina et al.*, 2000; *Tsurutani et al.*, 2001c]. The characteristics of wave modes will be studied in future.

[21] The DMSP F12 and F14 satellites crossed the dawnside auroral oval at ~20 min prior to and after the shock arrival. The MLT locations were ~2–3 hr earlier than the FAST locations. The satellite orbits, observations of magnetic field variations, electron energy flux, and electron energy spectrum are shown in Figure 3 from top to bottom. In Figure 3a, F12 crossed the auroral oval from ~0917 to 0922 UT during which the solar wind, magnetosphere and ionosphere were in a very quiet state (see Figure 1a). The maximum downward electron flux above the main auroral oval (from 0919 to 0921 UT) was ~0.4 erg cm^{-2} s^{-1} sr^{-1}, which is lower than the threshold for causing visible aurora (a value of ~1.0 erg cm^{-2} s^{-1} sr^{-1} at DMSP altitudes). The electron energy was ~4 to 7 keV in this region as shown in the bottom panel.

[22] Between 1003 and 1009 UT F14 crossed the same local time region of the previous F12 crossing as shown in the orbit plot in Figure 3b. The magnetic field variations increased significantly. Since the satellite were crossing the field-aligned currents in the Southern Hemisphere and the B_y component is along the satellite velocity vector and B_x is toward nightside, the decreases in ΔB_x and ΔB_y show the effects upward field-aligned currents. The particle precipitation increased significantly during the time between the two passes. The electron energy flux increased to ~1.1 erg cm^{-2} s^{-1} sr^{-1} or higher, an increase of a factor of ~3. The electron energy spectrum shows that high-energy electrons with energies at ~4–8 keV were mainly at lower latitudes from ~66° to 71° MLAT. These electrons filled the loss cone, and Therefore were lost in the ionosphere. The energy flux was fairly constant along the path. On the other hand, the low-energy electron (<~1 keV) precipitation was mainly in the high-latitude region from ~71° to 73.4° MLAT along the upward field-aligned currents as shown by the vertical shadings where there were ΔB_x and ΔB_y decreases and distinct energy fluxes. There is also an overlap region of ~71°–72.8° MLAT, within which high- and low-energy electrons (with energy flux above $\sim 3 \times 10^4$ keV/cm^2 sr eV) were detected simultaneously. This electron distribution structure is very similar to that observed at FAST in a nearby local time region.

3.2. The 4 August 1997 Event

[23] An interplanetary pressure pulse event that occurred on 4 August 1997 and its auroral effects are shown in Figure 4. Figure 4a shows the solar wind observations when Wind was at (84, −62, −2 R_e) and the geomagnetic AL index. The solar wind data have been shifted 20 min to adjust for the solar wind convection from Wind to the nose of the magnetopause (assuming a distance of 10 R_e). The time at the top is the time at Wind. The shifted time will be used for the data description and discussion in the follow-

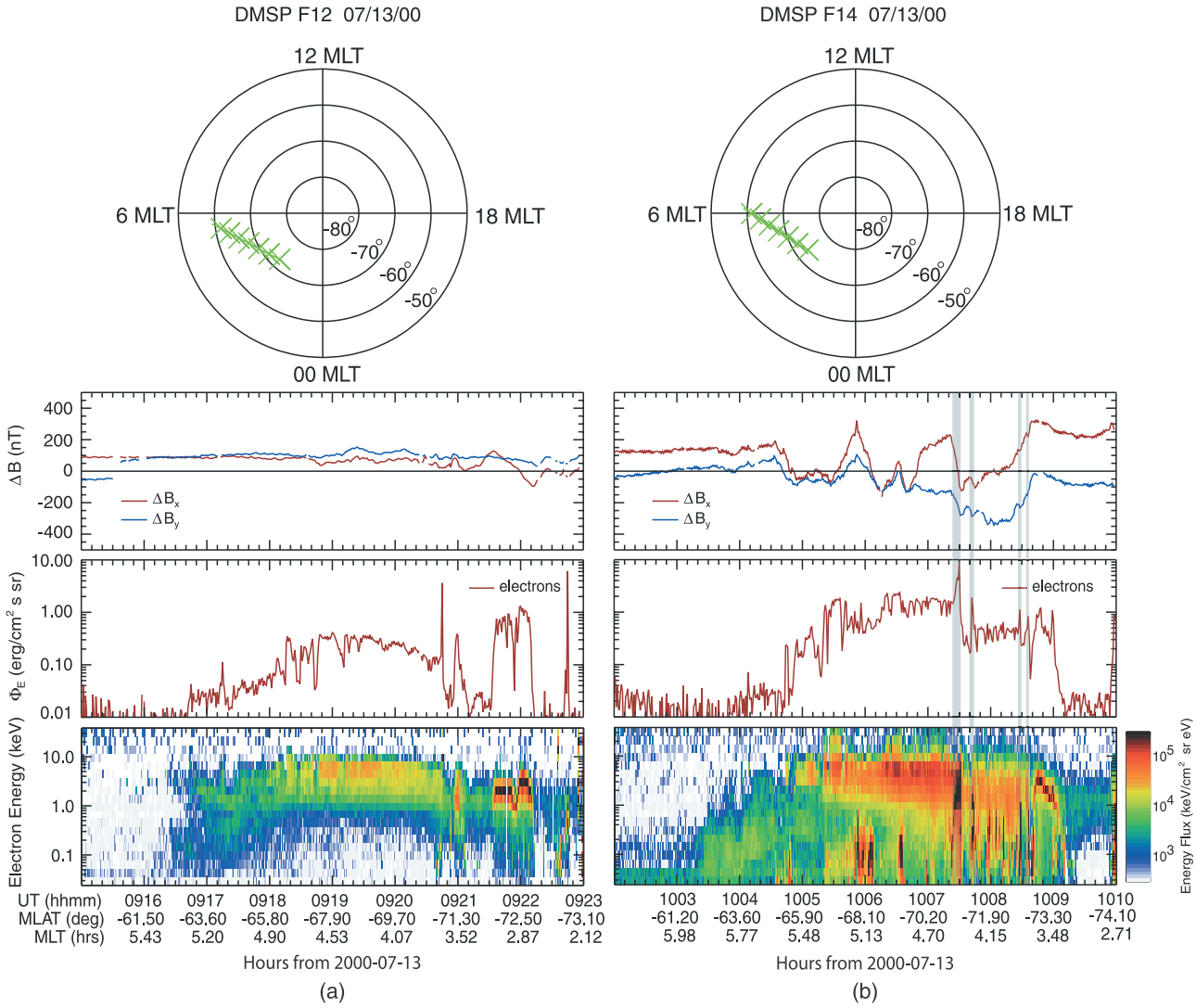

Figure 3. DMSP observations for the 13 July 2000 event during a dawnside auroral zone pass in the Southern Hemisphere. DMSP satellites are at ~840 km altitude. Satellites F12 and F14 locations are shown by the green crosses in the orbit plots at the top. The orbits are shown in magnetic coordinates. Figure 3a shows the observations during the F12 pass above the auroral oval prior to the shock arrival. Figure 3b shows the observations during the F14 pass after the arrival.

ing. Wind observed the pressure pulse at ~0235 UT when the solar wind ram pressure increased from ~5 to 10 nPa. The IMF B_z component was northward at ~5 nT for the entire interval shown in Figure 4a. The lowest AL was −107 nT at ~0110 UT.

[24] Figure 4b shows the Polar UVI images acquired during two FAST passes of the dawnside auroral oval in the Northern Hemisphere. In this study we mainly used two of four filters of the UV imager. They are the Lyman-Birge-Hopfield (LBH) short-wavelength filter centered at ~150 nm and the LBH long-wavelength filter centered at ~170 nm [*Torr et al.*, 1995]. The locations of the FAST foot points are shown by the centers of the small circles in the images when the FAST observations are shown in Figure 5. The images in the top two rows are for the FAST pass prior to the shock arrival. There were dayside auroras in both the dawnside and duskside auroral oval. These dayside auroras may have been caused by the relatively high ram pressure (4–5 nPa). The cusp aurora was in the 1200–1600 MLT sector above 80° MLAT. There was auroral activity in the duskside polar cap that may be associated with the northward IMF B_z and the strong positive IMF B_y [*Davis*, 1963; *Meng*, 1981; *Hardy et al.*, 1986; *Newell and Meng*, 1995], and with the ionospheric convection driven by the lobe reconnection [*Eriksson et al.*, 2002]. In the dawnside sector there were no obvious auroral intensity variations. The intensity remained at ~1 kR throughout the FAST crossing. The images in the bottom two rows show that the shock aurora occurred at ~0235 UT (after a comparison with the auroral enhancement shown in the Polar UVI LBHL images). At 0236:53 UT, noon and dawnside auroral brightening increased. At 0239:57 UT the auroral brightening was at ~2 kR in the 0900–1200 MLT sector between 72° and 80° MLAT. The aurora near local noon had expanded to low latitudes to ~65° MLAT, which is consistent with the *Liou et al.* [2002] results about midday subaurorae caused by

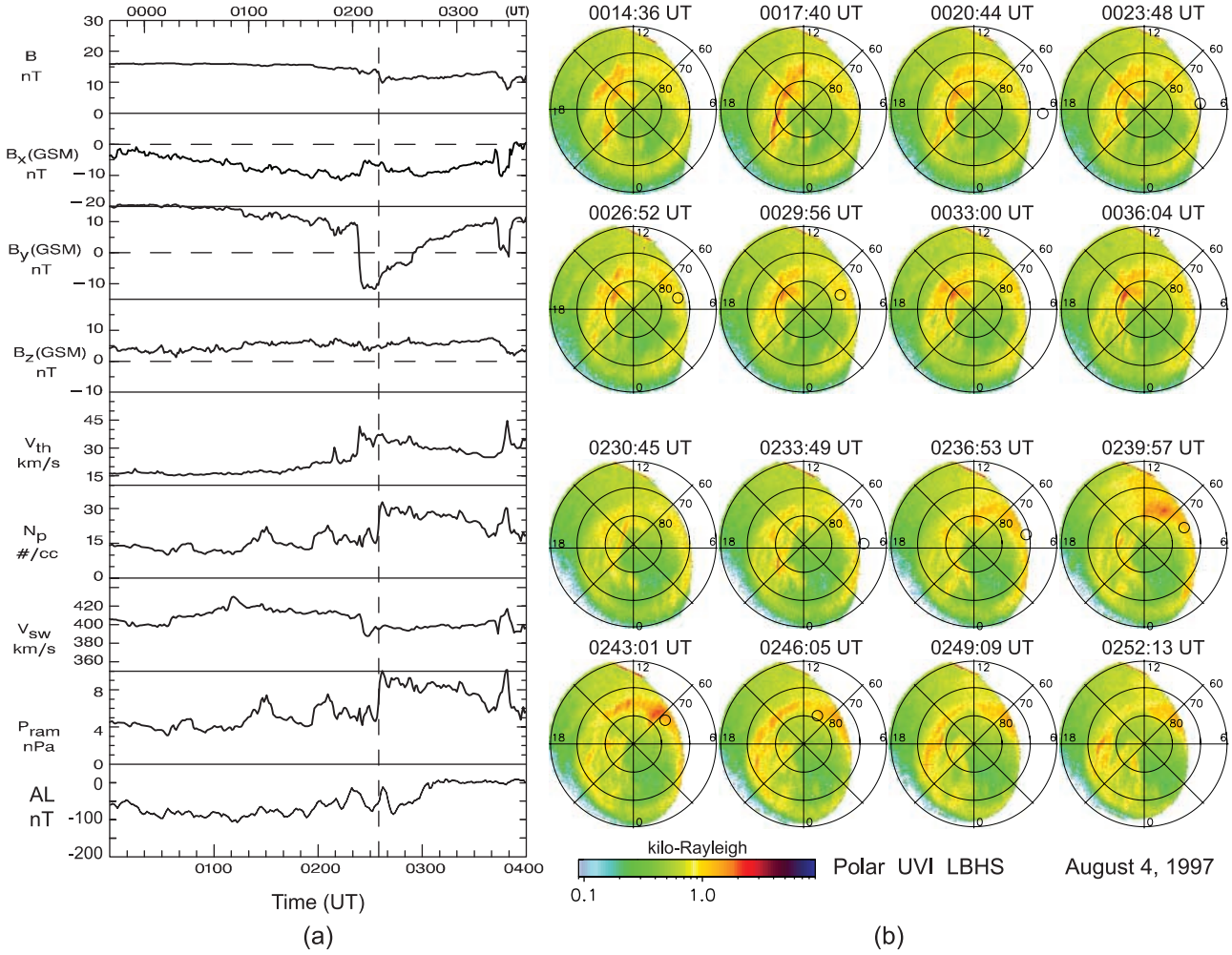

Figure 4. (a) Wind observations and the AL index for the 4 August 1997 solar wind ram pressure pulse event. The solar wind data have been shifted 20 min for the time delay as the solar wind propagated from Wind to the nose of the magnetopause (10 R_e). The time at the top is the time at the Wind spacecraft. (b) The auroral borealis observed by the Polar UVI prior to and after the pressure pulse arrival at the Earth at ~0035 UT on 4 August 1997. The aurora is shown in geomagnetic coordinates. In each image the magnetic pole is in the center, magnetic local noon is at the top, dawn is on the right. The time sequence goes from left to right, then down to the next row. The cadence of the images is ~3 min. The centers of the small circles in the images from 0020:44 to 0029:56 UT and from 0233:49 to 0246:05 UT are the FAST locations at the corresponding times. The images in the top two rows show the aurora and FAST locations as FAST crossed the dawnside oval in the orbit prior to the pressure pulse arrival. The images in the bottom two rows show the aurora and FAST locations as FAST crossed the dawnside oval right after the arrival.

interplanetary shocks. The auroral intensity was at ~1 kR from ~65° to 73° MLAT and decayed shortly thereafter and disappeared at 0243:01 UT. The auroral intensity at the poleward boundary of the dawnside oval was ~1.3–1.8 kR. The duskside auroral intensity increased at this time and expanded into the nightside oval as shown in the next two images at 0246:05 and 0249:09 UT, respectively.

[25] The FAST orbits and observations for the 4 August 1997 event are shown in Figure 5, which has the same format as Figure 2. FAST crossed the dawnside auroral oval between ~0020 and 0031 UT as shown in Figure 5a. FAST encountered upward region 2 field-aligned currents from ~0023 (~70°) to 0028 UT (75° ILAT), and then downward region 1 currents to 0031 UT (78° ILAT), as shown by the ΔB_E decrease from ~0 to −200 nT and then the increase to 250 nT. The current density is lower in the region 2 area than in the region 1 area. The electrons precipitating in the current regions were mainly at an energy level lower than 1 keV.

[26] FAST crossed the dawnside oval from 0232 to 0247 UT around the shock arrival at ~0235 UT. The observations are shown in Figure 5b. The convection pattern was modified as shown by the changed magnetic field in the orbit plot. FAST crossed the region 2 field-aligned current between ~0239 UT at ~73° ILAT and ~0243 UT at ~76° ILAT as the ΔB_E component decreased from ~70 to −100 nT, and then crossed the region 1 current till ~0246 UT at ~79° ILAT as ΔB_E increased from ~−100 to 200 nT. The calculated current density based on ΔB_E did not increase

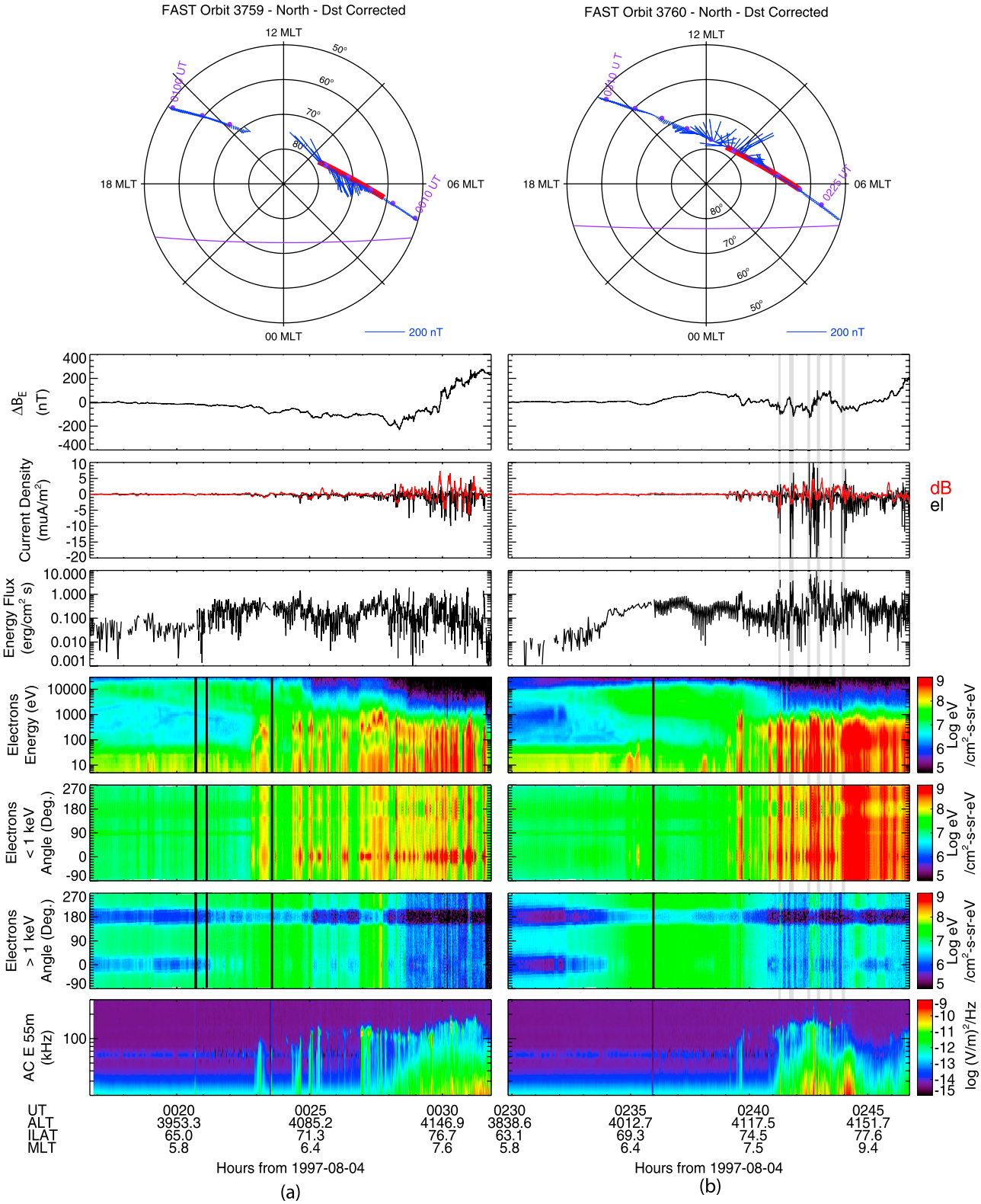

Figure 5. FAST observations for the 4 August 1997 event. FAST crossed the dawnside auroral zone in the Northern Hemisphere during this event. Figure 5 has the same format as Figure 2. Figure 5a shows the observations of orbit 3759 above the auroral oval prior to the pressure pulse arrival. Figure 5b shows the observations of orbit 3760 above the auroral oval after the arrival.

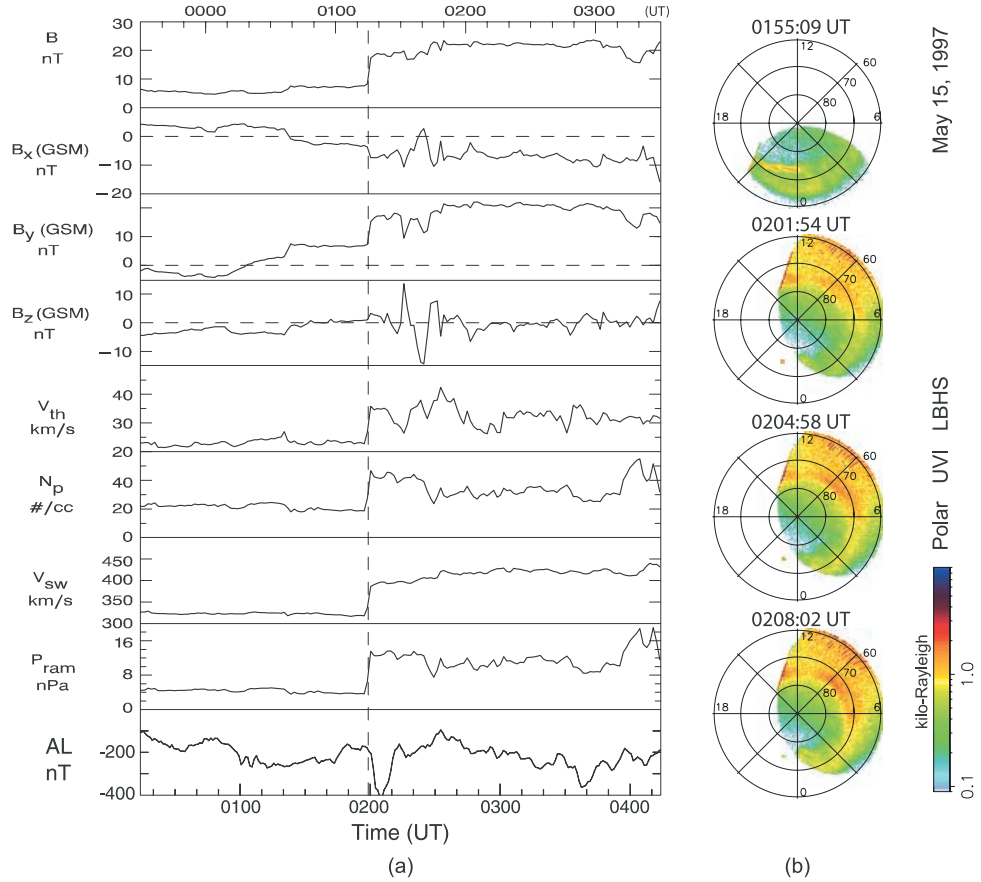

Figure 6. (a) Wind observations and the AL index for the 15 May 1997 interplanetary shock event. Figure 6a has the same format as Figure 4a. The solar wind data have been shifted 44 min. (b) The shock aurora observed by the Polar UVI instrument. The auroral brightening was caused by the interplanetary shock shown in Figure 6a. The LBHS (150 nm) images were used to show the auroral intensification. The aurora is shown in geomagnetic coordinates. The time sequence goes from top to bottom. The image cadence is ~3 min, but there is a gap between the top two images due to a pointing adjustment of the instrument platform.

compared to that shown in Figure 5a, but the current density based on the electron precipitation increased significantly in both directions. The vertical shadings show that the electron precipitation increased obviously where there were upward field-aligned currents. These electrons were mainly at the higher latitude region of 74°–79° ILAT and had energies less than ~1 keV as seen in the panels of electron energy spectrogram and the pitch angle distribution for energy <1 keV. In the panels of electron energy spectrum and pitch angle distribution for energy >1 keV, on the other hand, it is shown that the precipitation of electrons with energies higher than ~1–10 keV was mainly at lower latitudes from ~65° to 75° ILAT. The precipitating electrons were highly isotropic and filled the loss cone from ~68° to 75° ILAT. There is a small overlap region of low- and high-energy electron precipitation at ~74°–75° ILAT.

4. Interplanetary Shock Effect Observed by DMSP Above Auroral Zone

[27] An interplanetary shock was detected by the Wind instruments at (119, −4, 18 R_e) at ~0115 UT on 15 May 1997 and is denoted by the vertical dashed line in Figure 6a. The solar wind data have been shifted 44 min for the time delay from Wind to the nose of the magnetopause. The time at the top of Figure 6a is the time at Wind. The IMF B_z was near zero for ~30 min in the shock upstream region. At the shock the ram pressure increased by ~10 nPa. The AL was ~−250 nT for one hour before the shock arrival, which may be associated with the small negative IMF B_z before 0120 UT. The AL index decreased to ~−400 nT after the shock arrival at ~0206 UT and remained largely negative for only ~10 min. The ground magnetograms in the Image chain have shown that the maximum H component decrease was ~220 nT at station Soroya (SOR). SOR was at ~67° MLAT and ~5 MLT at 0200 UT. At magnetic midnight, the maximum H component decrease at the Greenland chain was 190 nT at station Narsarsuaq (NAQ), which is at ~71° MLAT. The maximum H component decrease at the CANOPUS stations was ~100 nT at the Eskimo Point (ESKI) station at ~69° MLAT and 1930 MLT. The above observations indicate that this AL index decrease after the shock arrival was not caused by a substorm, but the enhanced dayside westward current due to the shock compression.

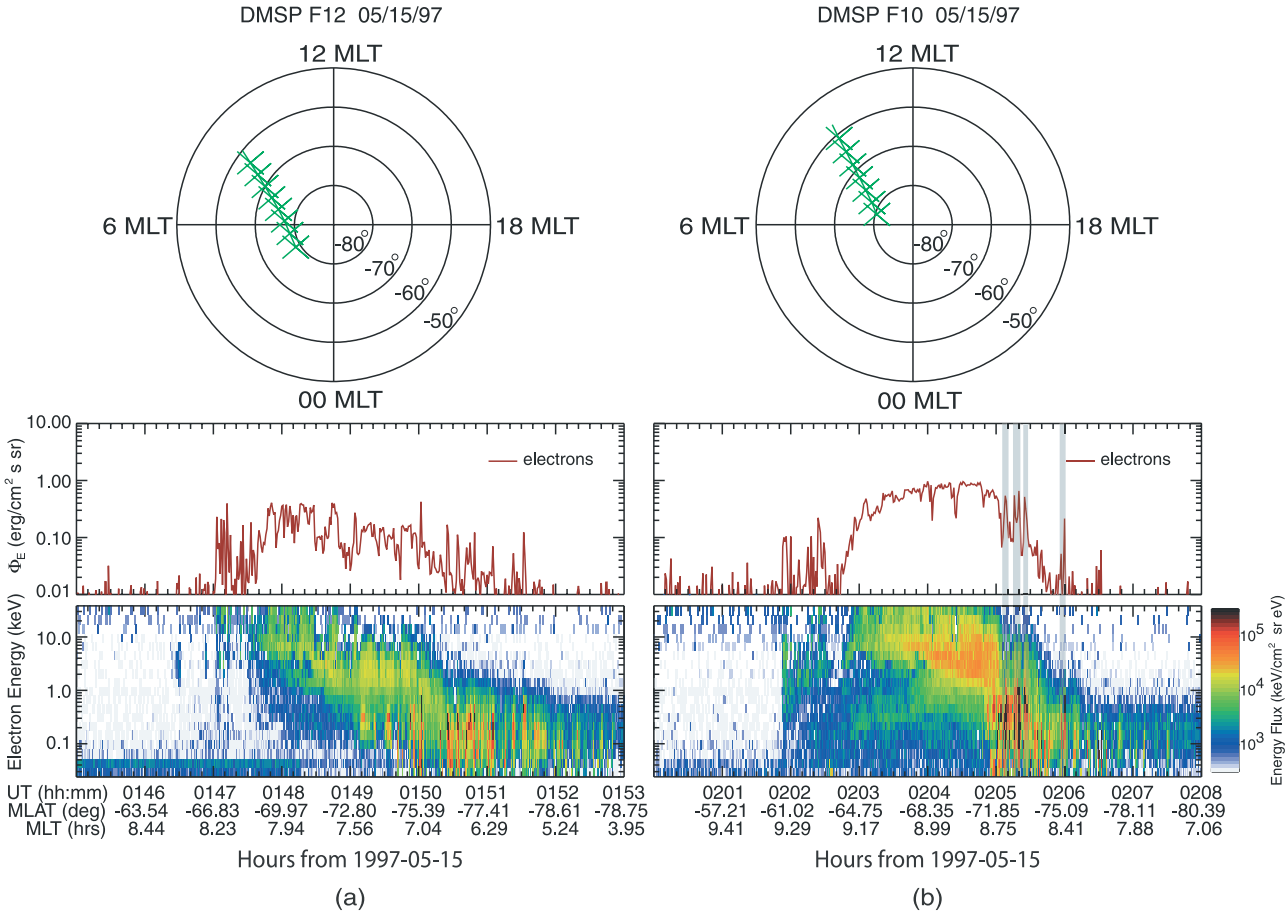

Figure 7. DMSP observations for the 15 May 1997 event during a dawnside auroral zone pass in the Southern Hemisphere. Figure 7 is formatted the same as Figure 3. Figure 7a shows the F12 observations ~7–12 min prior to the shock arrival. Figure 7b shows the F10 observations ~3–7 min after the shock arrival.

[28] Figure 6b shows the Polar UV images for the auroral intensification caused by this interplanetary shock. There are no LBHS (with 36.7 sec exposure time) images between 0155:09 and 0201:54 UT because of the view pointing adjustment of the instrument platform. The shock arrived at Earth at ~0159 UT as shown by the SSC. The image at 0201:54 UT shows that the dayside auroral brightness was ~1 kR in the 0600–1200 MLT sector and increased to ~2 kR at 0900 MLT at 0208:02 UT. The dayside aurora also expanded from 0600 MLT at 0201:54 UT to 0040 MLT at 0208:02 UT.

[29] Figure 7a shows that the DMSP satellite F12 crossed the dawnside auroral oval in the Southern Hemisphere from ~0147 to 0152 UT, ~7–12 min prior to the shock arrival at the Earth. Within 5 min after the shock arrival F10 crossed almost the same location as the F12 pass (see the orbit plots at the top). Figure 7b shows that downward electron energy flux increased about a fact of 2 with a maximum of ~1 erg cm^{-2} s^{-1} sr^{-1}. The electron energy spectrum shows that at lower latitudes from ~65° to 72° MLAT, the increased energy flux was mainly caused by the high-energy electron (2–8 keV) precipitation; at higher latitudes from ~72° to 75° MLAT, the increased energy flux was mainly caused by low-energy electrons (<~1 keV). The energy flux of the high-energy electron precipitation was fairly constant along the satellite path. While the energy flux of the low-energy electron precipitation was highly structured as shown by the vertical shadings where there are spikes of electron energy fluxes. There were no SSM data from F10 for this event, so we can't show whether there were upward currents at the spikes. However, the FAST observations and the DMSP data in Figure 3 have shown that spikes of the energy flux for low-energy electrons are highly correlated to the upward field-aligned currents. The overlap region of the high- and low-energy electron precipitation was less than 1° MLAT at ~71° MLAT. This is the same structure as shown in the FAST observations in Figures 2 and 5. This structure has been seen in all events of the dawnside sector crossings in Table 2.

5. Possible Mechanisms of Particle Precipitation and Auroral Forms

5.1. Field-Aligned Current Intensification and Low-Energy Electron Precipitation

[30] The instruments on board the FAST and DMSP satellites have detected that within ~10 min after shocks/pressure pulses arrived at the Earth, the field-aligned current density increased mainly in the high-latitude boundary of

the dawnside and duskside auroral oval where there were measurements. Precipitating electrons along those field-aligned currents were mainly at lower energies (<~1 keV). Broadband wave intensity (the E component) also increased on the magnetic field lines where the field-aligned currents were detected. This observation indicates that the solar wind-magnetosphere interaction increased significantly at the magnetopause boundary as shocks/pressure pulses compressed and squeezed the magnetopause. In the following sections, several possible mechanisms that may have contributed to the field-aligned current generation will be discussed.

5.1.1. Magnetic Field Shearing

[31] As shocks/pressure pulses squeeze the magnetopause and propagate antisunward, the magnetic field lines in the magnetopause and magnetopause boundary layers may be dragged tailward with the shock. Therefore magnetic shearing may occur between those distorted magnetic field lines and the field lines at lower L shells. *Haerendel* [1994] has shown that this magnetic shearing can generate field-aligned currents due to the decoupling of the plasma, which allows fast stress relief. The generation of the unstable field-aligned currents is a process that converts energy stored in magnetic shear stresses initiated from the shock compression into kinetic energy.

[32] This theory allows evaluation of the magnitude of the parallel potential drops using simple expressions, such as the ''Knight'' relationship:

$$j_{\parallel} = K\Phi_{\parallel}, \tag{1}$$

where $K^{-1} = \pi^{1/2} m_e C_{BL}/e^2 n_{BL}$ is the mirror impedance [*Haerendel*, 2001], and m_e, C_{BL}, e and n_{BL} are the electron mass, electron thermal speed in the boundary layer (BL), the electron charge and the plasma density in the BL. We can assume a field-aligned current focusing from the LLBL to the ionosphere:

$$j_{\parallel} = j_{\parallel BL}\, B_{IO}/B_{BL}, \tag{2}$$

where B_{IO} and B_{BL} are the field magnitudes of the ionosphere and BL, while $j_{\parallel BL}$ is the parallel current in the BL associated with the perturbation magnetic field $\Delta B_{\perp BL}$ and is determined by virtue of Ampère's law:

$$j_{\parallel BL} = \Delta B_{\perp BL}/\mu_o W_{BL} \tag{3}$$

where W_{BL} is the width of the BL. We have used the measured values of the BL (B_{BL} = 30 nT, n_{BL} = 10 cm^{-3}, C_{BL} = 6000 km s^{-1} if the electron temperature is 100 eV), W_{BL} is ~2000 km, and $B_{IO} = 0.5 \times 10^5$ nT. Assuming a perturbation field of $\Delta B_{\perp BL}$ = 20 nT, a potential of ~0.5 kV was derived, which is a very reasonable value of electron energy for producing discrete auroras. Furthermore, the energetic electrons observed at FAST and DMSP were typically less than 1 keV in energy.

[33] As a consistency check we shall compare the field-aligned current density and magnetic field perturbation as assumed for the boundary layer with FAST observations. From equation (3) the current density at the boundary layer should be 0.01 μA/m^2. We can relate this current density to that at FAST altitudes by the magnetic field ratio. For the events discussed here, the FAST altitude was ~2500 km, and B_o is ~20,000 nT. Assuming that the ambient field in the boundary layer is ~30 nT, the field aligned current density at FAST should be ~6.7 μA/m^2. The current density implied by the FAST magnetic field data is ~5 μA/m^2 associated with the electron burst at 0956:40 UT on orbit 15435 (Figure 2). The perturbation field maps approximately as the square root of the magnetic field ration and should be ~25 times bigger at FAST, i.e., ~500 nT. The observed ΔB is about 200 nT. Thus the values used for the calculation of equations (1)–(3) are acceptable, although somewhat on the high side in comparison to the observations.

5.1.2. Alfvén Wave Generation

[34] In a plasma environment of a compressible, non-viscous, perfectly conducting fluid immersed in a magnetic field, the momentum equation shows that the pressure gradient is a source of plasma motion. Three solutions of the dispersion relation obtained from the momentum equation are the shear Alfvén waves, fast and slow waves [*Bittencourt*, 1995; *Kivelson and Russell*, 1995].

[35] Magnetic field bending is carried by the shear Alfvén waves, while pressure gradients are carried by the fast-mode waves. Plasma flow across the field can increase the bending of the field, then generate the shear Alfvén waves and field-aligned currents. Particles that are precipitated along these field-aligned currents may cause auroras, so that the aurora would be observed at all latitudes where the shear Alfvén waves occur. The shock aurora propagation speed would be the Alfvén wave speed. If we use B ≈ 50 nT for the magnetic field just inside the magnetopause, and a plasma density $N_p \approx$ 1 cm^{-3}, the Alfvén waves can propagate at a speed of ~1000 km s^{-1} in the magnetosphere, and arrive at the nightside plasma sheet within 2 min. This implies that the shock aurora, if it is generated by these Alfvén waves, can reach the midnight sector in ~1–2 min or faster. Some shock aurora events, such as 24 September 1998 [*Zhou and Tsurutani*, 2001], do show that the aurora propagated at very high speed and reached the midnight sector 1–2 min after the shock arrived at the nose of the magnetopause. However, fast-mode waves radiate away into the magnetosphere from the boundary source near the nose of the magnetopause where it is first impinged upon by shocks/pressure pulses (see Figure 9). It is not known at this time why the field-aligned currents and aurora only occur in a constrained latitudinal region, while these waves are generated in all the L shells.

5.1.3. Magnetopause Perturbations

[36] *Southwood and Kivelson* [1990] and *Glassmeier and Heppner* [1992] have considered the field-aligned currents generated when step-function variations in the solar wind ram pressure impinge on the magnetopause/magnetosphere. The authors emphasized that in some regions within the magnetosphere, such as the inner edge of the LLBL and the outer edge of the plasmasphere, the fast mode waves generated in a way described above are capable of carrying currents to the ionosphere. Whereas *Southwood and Kivelson* [1990] predicted that each step-function change in the solar wind ram pressure will launch a pair of oppositely directed field-aligned currents into the ionosphere, *Glassmeier and Heppner* [1992] claimed that there will be only one field-aligned current.

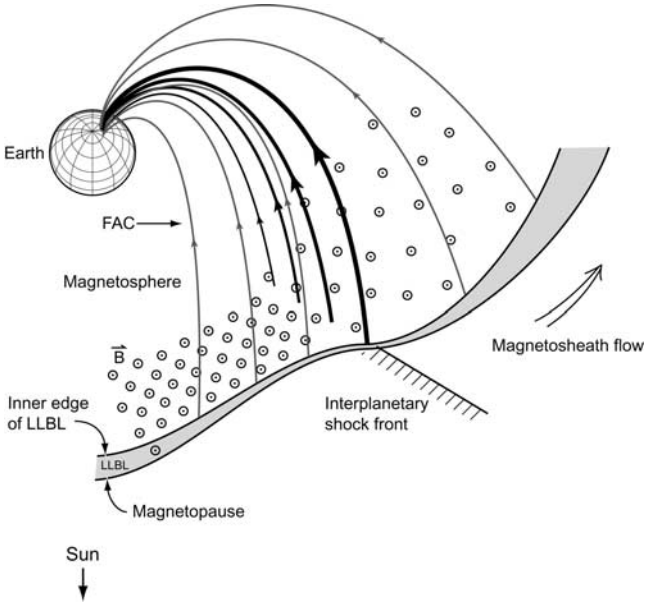

Figure 8. Field-aligned currents generated at where there is an azimuthal magnetic field gradient as described by equation (5). The currents are shown by arrowed thick solid lines. The decrease of the line thickness indicates a current density decrease as the pressure gradient decreases toward the Earth.

[37] We can derive the field-aligned current density by taking the divergence of the current perpendicular to the magnetic field, itself derived from the momentum equation:

$$J_{//} = -\int_{s=0}^{s} \nabla_{\perp} \cdot \left[\mathbf{B} \times \left(\rho \frac{d\mathbf{V}}{dt} + \nabla_{\perp} p \right) / B^2 \right] ds \qquad (4)$$

[38] We have obtained a simple, but exact, solution for the field-aligned currents generated by a pressure pulse compressing the magnetopause by linearizing equation (4), invoking the pressure balance condition for 0-order quantities ($p_o + B_o^2/2\mu_o$ = constant), using the polytropic gas law ($p_o = 1/\rho_o^{\gamma}$), for $\gamma = 5/3$, and employing a moderate amount of algebraic manipulation:

$$J_{1//} = -\frac{2}{B_o^2} \frac{\partial \rho_o}{\partial x} \int_{z=0}^{z} \frac{\partial B_{1z}}{\partial y} dz \qquad (5)$$

where the integral is taken along the field line from the equator to the ionosphere. Equation (5) demonstrates explicitly that field-aligned currents are generated when an azimuthal magnetic field gradient is applied to a 0-order radial gradient in the plasma parameters.

[39] The origin of this field-aligned current is easy to understand. An azimuthal current flowing along the inner edge of the LLBL separates the LLBL from the magnetosphere proper. When and where the magnetosphere is compressed, this current increases. As illustrated in Figure 8, current closure at the boundary between compressed and unperturbed regions requires field-aligned currents. In the particular example shown, it requires a downward field-aligned current on the leading edge of the compression. The corresponding ionospheric signature would be a single vortex, propagating antisunward. Such vortices are known to be associated with transient auroras [*Vorobjev*, 1994; *Luhr et al.*, 1996].

[40] This model explains two aspects of the shock aurora observations. First, the field-aligned currents lie just inside the magnetopause. They therefore map to the polarward boundaries of the dawnside and duskside auroral oval, which is consistent with the FAST and DMSP observations shown in Sections 3 and 4. Second, the auroras associated with the field-aligned currents should propagate antisunward along the oval in the ionosphere at the same angular speed as the magnetosheath flow at which the ram pressure variations move tailward on the magnetopause. The consistency of the shock aurora propagation speed and the near Earth solar wind speed has been reported by *Zhou and Tsurutani* [1999].

5.1.4. Magnetic Reconnection

[41] Another possible mechanism for field-aligned current intensification at the L shell that maps to the poleward boundary of the dayside auroral oval is dayside magnetic reconnection that occurs more intensely and frequently with interplanetary shocks/pressure pulses [*Song and Lysak*, 1994]. Fast forward interplanetary shocks compress magnetic fields upstream of the shock. To first order, the directionality of the fields is conserved. Thus, if the upstream field has a southward component, this component will be intensified by the shock (approximately by the magnetosonic Mach number). Also, the enhanced ram pressure leads to the formation of a number of magnetically compressed regions. If this increased ram pressure is strong enough, the magnetopause current sheet will become locally very thin. Reconnection can easily occur in these regions. Consequently, a patchy and intermittent interaction between the solar wind and the magnetopause, called driven and localized reconnection, will occur [*Song and Lysak*, 1994]. The reconnection rate is therefore a function of both the IMF strength and direction, and the solar wind ram pressure.

[42] A single twisted flux tube contains a helicity of $K = T\Phi^2$, where T is the (signed) number of twists and Φ is the flux in the tube [*Moffatt*, 1978]. The magnetic helicity is an approximate constant of motion during localized reconnection [*Berger*, 1984]. This fact has been used to explain the generation of field-aligned currents [*Song and Lysak*, 1989; *Wright and Berger*, 1989] which have the sense of the region 1 current system.

[43] The patchy and intermittent reconnection should occur primarily near local noon where the solar wind impinges most directly against the magnetopause. Therefore the field-aligned currents generated by reconnection would only be the most intense in a region of the magnetopause that maps to the poleward boundary of the dayside auroral oval near local noon where midday auroral breakups have been found [*Lockwood et al.*, 1989; *Sandholt et al.*, 1990]. Comparing the FAST observations for the 13 July 2000 (Figure 2) and 4 August 1997 (Figure 5) events, the latter one does show more intense field-aligned current effect when FAST was closer to the cusp region. However, the difficulty for explaining the

shock aurora propagation is how magnetic reconnection could occur only in the magnetopause where the shock/pressure pulse is compressing.

[44] Shock auroras occur even if the IMF B_z is northward (such as the 4 August 1997 event in Figure 4). Whether or not this signature is a negative indication of the reconnection contribution should be studied carefully in future, for dayside reconnection may still occur under northward IMF and may be controlled by the IMF B_y and B_x components [*Reiff and Burch*, 1985; *Crooker et al.*, 1998; *Sandholt et al.*, 2001; *Eriksson et al.*, 2002].

5.1.5. Velocity Shearing

[45] Growth rates for the Kelvin-Helmholtz (K-H) instability maximize for flow shears perpendicular to the magnetic field. Such shears occasionally occur at the magnetopause and frequently occur at the inner edge of the low-latitude boundary layer. Small perturbations on the magnetopause develop into waves [*Ogilvie and Fitzenreiter*, 1989]. Corresponding vortices have also been detected in auroral arcs [*Hallinan and Davis*, 1970; *Oguti*, 1974; *Connors and Rostoker*, 1993]. Vorticity associated with waves in the dusk (dawn) boundary layer generates localized upward (downward) field-aligned currents into both the northern and the southern polar ionospheres [*Wei and Lee*, 1993]. Discrete aurora in "beads" or "pearls" and SSC associated geomagnetic pulsations in both the dawnside and duskside high-latitude ionosphere have been attributed to the K-H instability [*Miura and Sato*, 1978; *Wagner et al.*, 1983; *Lui et al.*, 1989; *Potemra et al.*, 1990; *Connors and Rostoker*, 1993; *Shumilov et al.*, 1996].

[46] Because of ionospheric Joule dissipation, these vortices should survive less than ~10 minutes [*Kivelson and Chen*, 1995]. The vortices travel tailward with the phase velocity of the unstable K-H wave, which is nearly equal to half the magnetosheath flow speed [*Miura*, 1990]. The K-H instability-associated auroral brightenings could last longer (~10 min) behind propagating front edges than the auroral brightenings caused by the magnetopause perturbations. However, the auroral propagation speeds are slower than those of the auroras associated with the magnetic shearing, magnetopause perturbation and magnetic reconnection mechanisms.

5.2. Adiabatic Compression and High-Energy Electron Precipitation

[47] The instruments on board both FAST and DMSP satellites have also detected that within ~10 min after a shock/pressure pulse arrives at the Earth, high-energy electrons (~1–10 keV) precipitate mainly into the lower latitude region of the dawnside and duskside auroral oval. The increased electron energy flux might be a result of electron energization from lower energies. The particle energization due to interplanetary shock/pressure pulse compression could be caused by Betatron and Fermi acceleration [*Chamberlain*, 1961]. However, in the dayside magnetosphere the effect of magnetic field line shortening is much less than that of magnetic field strengthening. Therefore Fermi acceleration can be ignored compared to the Betatron acceleration effect that occurs in the dayside magnetosphere under compression conditions.

[48] Assuming the first adiabatic invariant is conserved where the shock compression occurs, the enhancement of the outer magnetospheric field leads to an increase of plasma heating in the perpendicular (to the magnetic field) direction and to a temperature anisotropy ($T_\perp/T_\parallel > 1$). The loss cone instability will result, leading to plasma wave growth, such as whistler mode waves [*Tsurutani et al.*, 1998]. Particles will be scattered into the loss cone and cause diffuse aurora at lower latitudes [*Zhou and Tsurutani*, 1999; *Tsurutani et al.*, 2001a, 2001b]. One would expect to see an enhancement of the ELF/VLF wave intensity, or the generation of ion cyclotron waves and whistler mode waves as the pitch angle diffusion occurs. However, the wave instabilities that cause pitch angle scattering have the strongest growth at the equator plane where minimum B occurs. Thus the waves are the most intense near the equatorial plane and a detection for the effect of the wave-particle interaction would rely highly on the correct time (when the compression occurs) and location (near the LLBL within the outer magnetosphere) of spacecraft observations.

5.3. Auroral Forms

5.3.1. Field-Aligned Currents and Discrete Auroras

[49] It was shown in Sections 3 and 4 that the downward electron energy flux was significantly high along the upward field-aligned currents (see figures of the FAST and DMSP observations), but was low between these current layers, where the currents were going downward. Therefore the aurora generated beneath the upward field-aligned current layers would be much brighter than that beneath the downward currents. Since those upward field-aligned current layers are very thin in the magnetic latitudinal directions, the aurora beneath them would have looked like discrete brightenings or arcs in the ionosphere, which depict the foot prints of the upward field-aligned currents.

[50] Field-aligned current relationship to auroral arcs can be analogous to an artificial fountain, in which water is ejected in layers. Water falls into the pond and makes splashes at the bottoms of the water layers. The traces of the splashes can be straight lines, circles, or curved shape depending on the design of the water layers. The size of the splashes would be determined by the amount and speed of the falling water.

[51] Although the electrons precipitated along the upward field-aligned currents are at low energies (<~1 keV), this does not necessarily imply a low auroral intensity, because the auroral brightening is determined by the strength of the energy flux instead of the energy level of individual electrons. Thus the auroral arcs can sometimes be very distinguishable, while at other times, they can be washed out by a bright background of diffuse auroras.

5.3.2. Adiabatic Compression and Diffuse Auroras

[52] Electrons lost into the loss cone due to the adiabatic compression as discussed above will precipitate into the atmosphere along magnetic field lines which foot points are uniform in the atmosphere. When the precipitating energy flux is high enough, auroras would be generated and seen as a structureless bright background, i.e., diffuse aurora. Particles escaping from the loss cone and causing the diffuse aurora can be analogous to the falling of raindrops with a

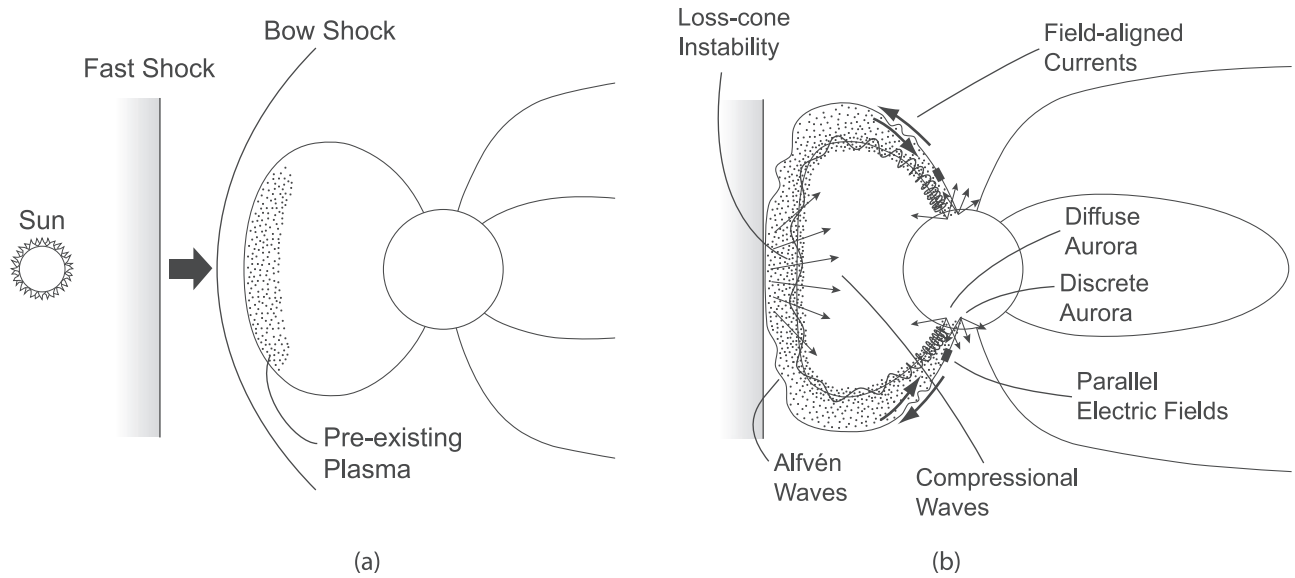

Figure 9. A schematic of possible phenomena in the dayside magnetosphere and ionosphere, which are generated by interplanetary shock/pressure pulse compression.

fairly uniform 2D distribution. Splashes of the raindrops are also uniform on the ground.

6. Summary and Conclusion

[53] In this paper we have shown that at ~4000 km, ~2000 km and 800 km altitudes, the FAST and DMSP instruments observed the same electron precipitation structures after interplanetary shock/pressure pulses impinged on the Earth's magnetopause. The signatures of the observations are the following.

[54] 1. Electron energy precipitation increased significantly in the dawnside and duskside auroral oval within ~10 min after the shock/pressure pulse arrived at the nose of the magnetopause. This effect explains the auroral intensity enhancements detected by the Polar UVI and the IMAGE FUV instruments.

[55] 2. The electron precipitation structure is of low-energy electrons ($\leq\sim$1 keV) at higher latitudes and high-energy electrons ($\sim$1–10 keV) at lower latitudes. There are a few degrees (1°–4° MLAT) of overlap between these two categories of precipitating electrons. The location of the overlap is along the boundary between the region 1 and 2 field-aligned currents.

[56] 3. The precipitation of the low-energy electrons was along highly structured field-aligned currents that might have generated electromagnetic broadband waves. The field-aligned currents were found to be mainly carried by electrons, which agrees with the results of *Carlson et al.* [1998]. These field-aligned currents were mainly at higher L shells than the high-energy electron precipitation. One would expect these low-energy electrons to produce discrete auroras in the poleward region of the auroral oval. The calculated parallel potential drop is ~0.5 keV, which is very close to the FAST and DMSP observations.

[57] 4. The precipitation of the high-energy electrons was highly isotopic with a filled loss cone. Therefore one would expect that the high-energy electrons create diffuse aurora in the lower latitude region of dawnside and duskside the auroral oval. These electrons may have preexisted in the magnetosphere before a shock arrived. They may have convected from the plasma sheet to the near Earth region, and then drifted to the dayside magnetosphere through the dawnside, due to the gradient and curvature of the geomagnetic field.

[58] Mechanisms for the above observations are discussed from the point of view of the solar wind-magnetosphere interaction under interplanetary shock/pressure pulse conditions, which includes intense magnetopause processes that may have generated field-aligned currents and dayside magnetopause/magnetosphere compression that may have created Betatron acceleration. A schematic that explains all mechanisms and phenomena discussed in this paper is shown in Figure 9, in which Earth and the magnetic field lines are shown in the noon-midnight meridional plane. The interplanetary shock normal is along the Sun-Earth connection line. Figure 9 shows that an intense impact of an interplanetary shock may generate Alfvén waves as well as loss cone instability, which may lead to two types of precipitations of particles preexisting in the outer magnetospheric region creating diffuse and discrete auroras as shown in Figure 9b.

[59] In conclusion, electron energy precipitation increases significantly after shock/pressure pulse arrivals, which causes dayside auroral intensification. The structure of the electron precipitation implies that dayside shock aurora consists of discrete auroras at higher latitudes and diffuse auroras at lower latitudes in general. The precipitation of low-energy electrons (which causes discrete auroras) is associated with the field-aligned currents generated by some magnetopause processes under shock/pressure pulse conditions, such as magnetic shearing, magnetopause perturbation, magnetic reconnection and/or Alfvén wave generation. The precipitation of high-energy electrons (which

causes diffuse auroras) is likely to be caused by the adiabatic compression.

[60] **Acknowledgments.** Portions of this research was performed at the Jet Propulsion Laboratory, California Institute of Technology, under contract with the National Aeronautics and Space Administration. The work by P. C. Anderson was supported by NASA grant NSF-ATM-0000268. We thank C. T. Russell for the helpful scientific discussions. The AL indices were provided by the World Data Center of Geomagnetism at Kyoto University, Japan. K. Ogilvie and R. P. Lepping provided the Wind SWE and MFI data. We thank the institutes who maintain the Image magnetometer array and DMI Greenland magnetograms. The data used in this study from the CANOPUS instrument array are constructed, maintained and operated by the Canadian Space Agency.

[61] Arthur Richmond thanks Per Evan Sandholt and Vyacheslav G. Vorobjev for their assistance in evaluating this article.

References

Berger, M. A., Rigorous new limits on magnetic helicity dissipation in the solar corona, *Geophys. Astrophys. Fluid Dyn.*, *30*, 79, 1984.

Bittencourt, J. A., *Fundamentals of Plasma Physics*, Pergamon, New York, 1995.

Brittnacher, M., et al., Global auroral response to a solar wind pressure pulse, *Adv. Space Res.*, *25*, 1377, 2000.

Brown, R. R., et al., Large-scale electron bombardment of the atmosphere at the sudden commencement of a geomagnetic storm, *J. Geophys. Res.*, *66*, 1035, 1961.

Bythrow, P. F., et al., Observational evidence for a boundary layer source of dayside region I field-aligned currents, Multiple auroral arcs and Birkeland currents, *J. Geophys. Res.*, *86*, 5577, 1981.

Carlson, R., et al., The Fast Auroral SnapshoT (FAST) mission, *Geophys. Res. Lett.*, *25*, 2013, 1998.

Chamberlain, J. W., *Physics of the Aurora and Airglow*, edited by J. V. Mieghen, Academic, San Diego, Calif., 1961.

Connors, M., and G. Rostoker, Source mechanisms for morning auroral features, *Geophys. Res. Lett.*, *20*, 1535, 1993.

Craven, J. D., et al., Global auroral responses to magnetospheric compressions by shocks in the solar wind: Two case studies, in *Solar Wind-Magnetosphere Coupling*, edited by Y. Kamide and J. A. Slavin, pp. 367–380, Terra Sci., Tokyo, 1986.

Crooker, N. U., J. G. Lyon, and J. A. Fedder, MHD model merging with IMF By: Lobe cells, sunward polar cap convection, and overdraped lobes, *J. Geophys. Res.*, *103*, 9143, 1998.

Davis, T. N., Negative correlation between polar cap visual aurora and magnetic activity, *J. Geophys. Res.*, *68*, 4947, 1963.

Egeland, A., W. J. Burke, N. C. Maynard, E. M. Basinska, J. D. Winningham, and C. S. Deehr, Ground and satellite observations of postdawn aurorae near the time of a sudden storm commencement, *J. Geophys. Res.*, *99*, 2095, 1994.

Eriksson, S., J. W. Bonnell, L. G. Blomberg, R. E. Ergun, G. T. Marklund, and C. W. Carlson, Lobe cell convection and field-aligned currents poleward of the region 1 current system, *J. Geophys. Res.*, *107*(A8), 1185, 10.1029/2001JA005041, 2002.

Fasel, G. J., J. I. Minow, R. W. Smith, C. S. Deehr, and L. C. Lee, Multiple brightenings of transient dayside auroral forms during oval expansions, *Geophys. Res. Lett.*, *19*, 2429, 1992.

Frey, H. U., S. B. Mende, T. J. Immel, S. A. Fuselier, E. S. Claflin, J.-C. Gérard, and B. Hubert, Proton aurora in the cusp, *J. Geophys. Res.*, *107*(A7), 1091, doi:10.1029/2001JA900161, 2002.

Glassmeier, K. H., and C. Heppner, Traveling magnetospheric convection twin-vortices: Another case study, global characteristics, and a model, *J. Geophys. Res.*, *97*, 3977, 1992.

Gurnett, D. A., and L. A. Frank, A region of intense plasma wave turbulence on auroral field lines, *J. Geophys. Res.*, *82*, 1031, 1977.

Gurnett, D. A., et al., Plasma wave turbulence at the magnetopause: Observations from ISEE 1 and 2, *J. Geophys. Res.*, *84*, 7043, 1979.

Haerendel, G., Acceleration from field-aligned potential drops, *Astrophys. J. Suppl. Series*, *90*, 765, 1994.

Haerendel, G., Auroral acceleration in astrophysical plasmas, *Phys. Plasmas*, *8*, 2365, 2001.

Hardy, D. A., et al., Precipitating electron and ion detectors (SSJ/4) on the block 5D/Flights 6-10 DMSP satellites: Calibration and data presentation, *Rep. AFGL-TR-84-0317*, Air Force Geophys. Lab., Hanscom Air Force Base, Mass., 1984.

Hardy, D. A., et al., The characteristics of polar-cap precipitation and their dependence on the interplanetary magnetic field and the solar wind, in *Solar Wind-Magnetosphere Coupling*, edited by Y. Kamide and J. A. Slavin, pp. 575–604, Terra Sci., Tokyo, 1986.

Hallinan, T. J., and T. N. Davis, Small scale auroral arc distortions, *Planet. Space Sci.*, *18*, 1735, 1970.

Kivelson, M. G., and S.-H. Chen, The magnetopause: Surface waves and instabilities and their possible dynamical consequences, in *Physics of the Magnetopause*, *Geophys. Monogr. Ser.*, vol. 90, edited by P. Song, B. U. O. Sonnerup, and M. G. Thomsen, p. 257, AGU, Washington, D. C., 1995.

Kivelson, M. G., and C. T. Russell, *Introduction to Space Physics*, Cambridge Univ. Press, New York, 1995.

Lakhina, G. S., B. T. Tsurutani, H. Kojima, and H. Matsumoto, "Broadband" plasma waves in the boundary layers, *J. Geophys. Res.*, *105*, 27,791, 2000.

Leontyev, S. V., et al., Dayside aurorae and their relation to other geophysical phenomena, *Planet. Space Sci.*, *40*, 621, 1992.

Liou, K., C.-C. Wu, R. P. Lepping, P. T. Newell, and C.-I. Meng, Midday sub-auroral patches (MSPs) associated with interplanetary shocks, *Geophys. Res. Lett.*, *29*(16), 1771, doi:10.1029/2001GL014182, 2002.

Lockwood, M., P. E. Sandholt, and S. W. H. Cowley, Dayside auroral activity and momentum transfer from the solar wind, *Geophys. Res. Lett.*, *16*, 33, 1989.

Luhr, H., et al., Multi-instrument ground-based observations of a traveling convection vortices event, *Ann. Geophys.*, *14*, 162, 1996.

Lui, A. T. Y., D. Venkatesan, and J. S. Murphree, Auroral bright spots on the dayside oval, *J. Geophys. Res.*, *94*, 5515, 1989.

Mende, S. B., et al., Far ultraviolet imaging from the IMAGE spacecraft: 2. Wideband FUV imaging, *Space Sci. Rev.*, *91*, 271, 2000.

Meng, C.-I., The auroral oval precipitation boundary during extremely quiet geomagnetic conditions, *J. Geophys. Res.*, *86*, 4607, 1981.

Miura, A., Kelvin-Helmholtz instability for supersonic shear flow at the magnetospheric boundary, *Geophys. Res. Lett.*, *17*, 249, 1990.

Miura, A., Kelvin-Helmholtz instability at the magnetospheric boundary: Dependence on the magnetosheath sonic Mach number, *J. Geophys. Res.*, *97*, 10,655, 1992.

Miura, A., and T. Sato, Shear instability: Auroral arc deformation and anomalous momentum transport, *J. Geophys. Res.*, *83*, 2109, 1978.

Moffatt, H. K., *Magnetic Field Generation in Electrically Conducting Fluids*, Cambridge Univ. Press, New York, 1978.

Murphree, J. S., R. D. Elphinstone, D. Hearn, and L. L. Cogger, Large-scale high-latitude dayside auroral emissions, *J. Geophys. Res.*, *95*, 2345, 1990.

Newell, P. T., and C.-I. Meng, Creation of theta-auroras: The isolation of plasma sheet fragments in the polar cap, *Science*, *270*, 1338, 1995.

Ogilvie, K. W., and R. J. Fitzenreiter, The Kelvin-Helmholtz instability at the magnetopause and inner boundary layer surface, *J. Geophys. Res.*, *94*, 15,113, 1989.

Oguti, T., Rotational deformations and related drift motions of auroral arcs, *J. Geophys. Res.*, *79*, 3861, 1974.

Potemra, T. A., H. Vo, D. Venkatesan, L. L. Cogger, R. E. Erlandson, L. J. Zanetti, P. F. Bythrow, and B. J. Anderson, Periodic auroral forms and geomagnetic-field oscillations in the 1400 MLT region, *J. Geophys. Res.*, *95*, 5835, 1990.

Rairden, R. L., and S. B. Mende, Properties of 6300-Å auroral emissions at south pole, *J. Geophys. Res.*, *94*, 1402, 1989.

Reiff, P. H., and J. L. Burch, IMF By-dependent plasma flow and Birkeland currents in the dayside magnetosphere: 2. A global model for northward and southward IMF, *J. Geophys. Res.*, *90*, 1595, 1985.

Rich, F. J., et al., Enhanced ionosphere-magnetosphere data from the DMSP satellites, *Eos Trans. AGU*, *66*, 513, 1985.

Russell, C. T., and R. C. Elphic, Initial ISEE magnetometer results: Magnetopause observations, *Space Sci. Rev.*, *22*, 691, 1978.

Sandholt, P. E., et al., Midday auroral breakup, *J. Geomagn. Geoelectr.*, *41*, 371, 1989.

Sandholt, P. E., M. Lockwood, T. Oguti, S. W. H. Cowley, K. S. C. Freeman, B. Lybekk, A. Egeland, and D. M. Willis, Midday auroral breakup events and related energy and momentum transfer from the magnetosheath, *J. Geophys. Res.*, *95*, 1039, 1990.

Sandholt, P. E., et al., Cusp/cleft auroral activity in relation to solar wind dynamic pressure, interplanetary magnetic field Bz and By, *J. Geophys. Res.*, *99*, 17,323, 1994.

Sandholt, P. E., C. J. Farrugia, S. W. H. Cowley, and M. Lester, Dayside auroral bifurcation sequence during By-dominated interplanetary magnetic field: Relationship with merging and lobe convection cells, *J. Geophys. Res.*, *106*, 15,429, 2001.

Sandholt, P. E., et al., *Dayside and Polar Cap Aurora*, Kluwer Acad., Norwell, Mass., 2002.

Shumilov, O., E. Kasatkina, O. Raspopov, T. Hansen, and A. Frank-Kamenetsky, Sudden-commencement-triggered pulsations at high latitudes and their sources in the magnetosphere, *J. Geophys. Res.*, *101*, 17,355, 1996.

Sibeck, D. G., A model for the transient magnetospheric response to sudden solar wind dynamic pressure variations, *J. Geophys. Res.*, *95*, 3755, 1990.

Sibeck, D. G., The magnetospheric and ionospheric response to solar wind dynamic pressure variations, in *Modeling Magnetospheric Plasma Processes*, *Geophys. Monogr. Ser.*, vol. 62, edited by G. R. Wilson, p. 1, AGU, Washington, D. C., 1991.

Sibeck, D. G., et al., Comprehensive study of the magnetospheric response to a hot flow anomaly, *J. Geophys. Res.*, *104*, 4577, 1999.

Sitar, R. J., et al., Multi-instrument analysis of the ionospheric signatures of a hot flow anomaly occurring on July 24, 1996, *J. Geophys. Res.*, *103*, 23,357, 1998.

Song, Y., and R. L. Lysak, Evaluation of twist helicity in FTE flux tubes, *J. Geophys. Res.*, *94*, 5273, 1989.

Song, Y., and R. L. Lysak, Alfvénon, driven reconnection and the direct generation of field-aligned current, *Geophys. Res. Lett.*, *21*, 1755, 1994.

Southwood, D. J., and M. G. Kivelson, The magnetohydrodynamic response of the magnetospheric cavity to changes in solar wind pressure, *J. Geophys. Res.*, *95*, 2301, 1990.

Spann, J. F., M. Brittnacher, R. Elsen, G. A. Germany, and G. K. Parks, Initial response and complex polar cap structures of the aurora in response to the January 10, 1997 magnetic cloud, *Geophys. Res. Lett.*, *25*, 2577, 1998.

Torr, M. R., et al., A far ultraviolet imager for the international solar-terrestrial physics mission, *Space Sci. Rev.*, *71*, 329, 1995.

Tsurutani, B. T., et al., Wave-particle interactions at the magnetopause: Contributions to the dayside aurora, *Geophys. Res. Lett.*, *8*, 183, 1981.

Tsurutani, B. T., J. K. Arballo, G. S. Lakhina, C. Ho, B. Buti, J. S. Pickett, and D. A. Gurnett, Plasma waves in the dayside polar cap boundary layer: Bipolar and monopolar electric pulses and whistler mode waves, *Geophys. Res. Lett.*, *25*, 4117, 1998.

Tsurutani, B. T., et al., Interplanetary shocks, magnetopause boundary layers and dayside auroras: The importance of a very small magnetospheric region, *Surv. Geophys.*, *22*, 101, 2001a.

Tsurutani, B. T., et al., Auroral zone dayside precipitation during magnetic storm initial phases, *J. Atmos. Sol. Terr. Phys.*, *63*, 513, 2001b.

Tsurutani, B. T., et al., Polar cap boundary layer waves: An auroral zone phenomenon, *J. Geophys. Res.*, *106*, 19,035, 2001c.

Vo, H. B., and J. S. Murphree, A study of dayside auroral bright spots seen by the Viking auroral imager, *J. Geophys. Res.*, *100*, 3649, 1995.

Vorobjev, V. G., Dynamics of Hall vortices in the daytime high-latitude area, *Geomagn. Aeron.*, *33*, 612, 1994.

Vorobjev, V. G., et al., Dynamics of day and night aurora during substorms, *Planet. Space Sci.*, *23*, 269, 1975.

Vorobjev, V. G., O. I. Yagodkina, D. G. Sibeck, K. Liou, and C.-I. Meng, Polar UVI observations of dayside auroral transient events, *J. Geophys. Res.*, *106*, 28,897, 2001.

Wagner, J. S., et al., Small-scale auroral arc deformations, *J. Geophys. Res.*, *88*, 8013, 1983.

Wei, C. Q., and L. C. Lee, Coupling of magnetopause-boundary layer to the polar ionosphere, *J. Geophys. Res.*, *98*, 5707, 1993.

Wright, A. N., and M. A. Berger, The effect of reconnection upon the linkage and interior structure of magnetic flux tubes, *J. Geophys. Res.*, *94*, 1295, 1989.

Zhang, Y., L. J. Paxton, T. J. Immel, H. U. Frey, and S. B. Mende, Sudden solar wind dynamic pressure enhancements and dayside detached auroras: IMAGE and DMSP observations, *J. Geophys. Res.*, *107*, 8001, doi:10.1029/2002JA009355, 2002 [printed *108*(A4), 2003].

Zhou, X.-Y., and B. T. Tsurutani, Rapid intensification and propagation of the dayside aurora: Large-scale interplanetary pressure pulses (fast shocks), *Geophys. Res. Lett.*, *26*, 1097, 1999.

Zhou, X.-Y., and B. T. Tsurutani, Interplanetary shock triggering of nightside geomagnetic activity: Substorms, pseudobreakups, and quiescent events, *J. Geophys. Res.*, *106*, 18,957, 2001.

P. C. Anderson, The Aerospace Corporation, Los Angeles, CA 90009, USA.

J. K. Arballo, B. T. Tsurutani, and X.-Y. Zhou, Jet Propulsion Laboratory, Pasadena, CA 91109, USA. (xiaoyan.zhou@jpl.nasa.gov)

H. U. Frey, Space Science Laboratory, University of California, Berkeley, CA 94720, USA.

G. Haerendel, International University of Bremen, D-28759 Bremen, Germany.

D. G. Sibeck, NASA Goddard Space Flight Center, Greenbelt, MD 20771, USA.

R. J. Strangeway, Institute of Geophysics and Planetary Physics, UCLA, Los Angeles, CA 90095, USA.